Opto-Electronic Advances

Supplementary information

April 2023, Vol. 6, No. 4

DOI: 10.29026/oea.2023.220034

Switching of K-Q intervalley trions fine structure and their dynamics in n-doped monolayer WS_2

Jiajie Pei[1,2], Xue Liu[3], Andrés Granados del Águila[3], Di Bao[3], Sheng Liu[3], Mohamed-Raouf AMARA[3], Weijie Zhao[3], Feng Zhang[1], Congya You[4], Yongzhe Zhang[4], Kenji Watanabe[5], Takashi Taniguchi[5], Han Zhang[1]* and Qihua Xiong[6]*

[1]Collaborative Innovation Center for Optoelectronic Science and Technology, International Collaborative Laboratory of 2D Materials for Optoelectronic Science and Technology of Ministry of Education and Guangdong Province, College of Optoelectronic Engineering, Shenzhen University, Shenzhen 518060, China; [2]College of Materials Science and Engineering, Fuzhou University, Fuzhou 350108, China; [3]Division of Physics and Applied Physics, School of Physical and Mathematical Sciences, Nanyang Technological University, Singapore 637371, Singapore; [4]College of Materials Science and Engineering, Beijing University of Technology, Beijing 100124, China; [5]Research Center for Functional Materials, International Center for Materials Nanoarchitectonics, National Institute for Materials Science, Tsukuba, Ibaraki 305-0044, Japan; [6]State Key Laboratory of Low Dimensional Quantum Physics and Department of Physics, Tsinghua University, Beijing 100084, China.

*Correspondence: H Zhang, E-mail: hzhang@szu.edu.cn; QH Xiong, E-mail: qihua_xiong@tsinghua.edu.cn

This file includes:

Supplementary information for this paper is available at https://doi.org/10.29026/oea.2023.220034

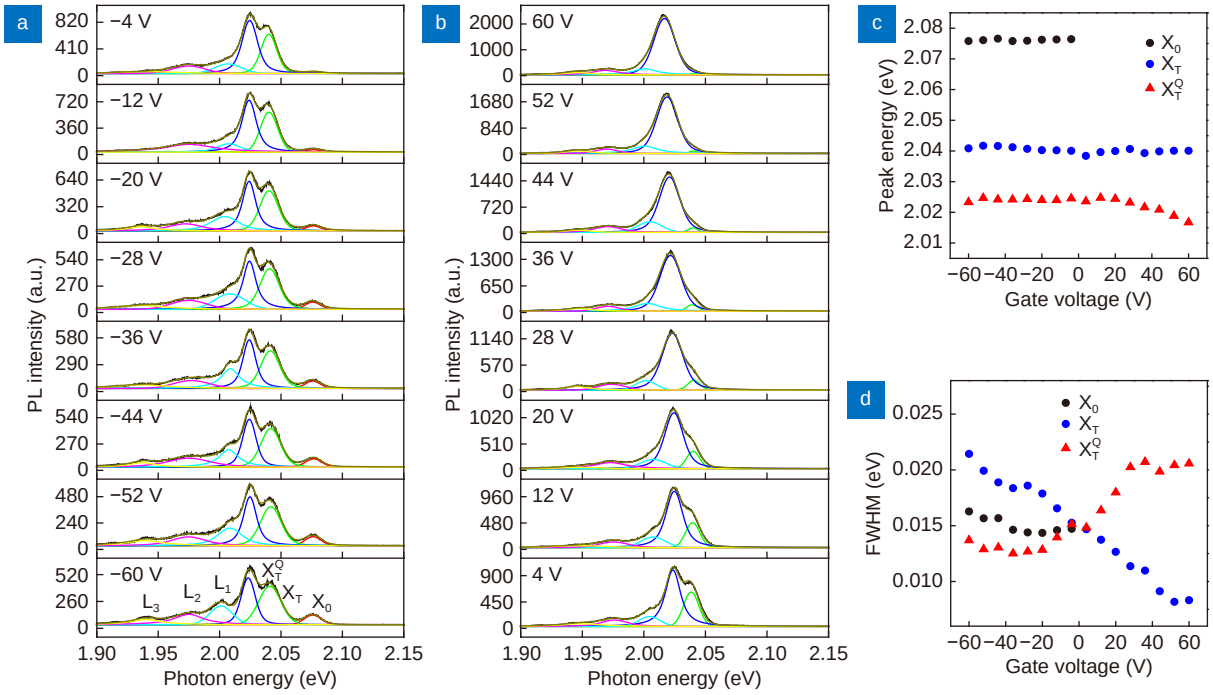

Fig. S1 | Fitting result of the gate-dependent PL spectra of the monolayer WS_2 taken at 10 K with a 25 μW excitation power. (**a**) Fitting result of the PL spectra from –60 V to –4 V back gate voltages with Voigt function. (**b**) Fitting result of the PL spectra from 4 V to 60 V back gate voltages with Voigt function. (**c**) PL peak energy of X_0, X_T, and X_T^Q emissions as a function of gate voltages. (**d**) Full width at half maximum (FWHM) of X_0, X_T and X_T^Q emissions as a function of gate voltages.

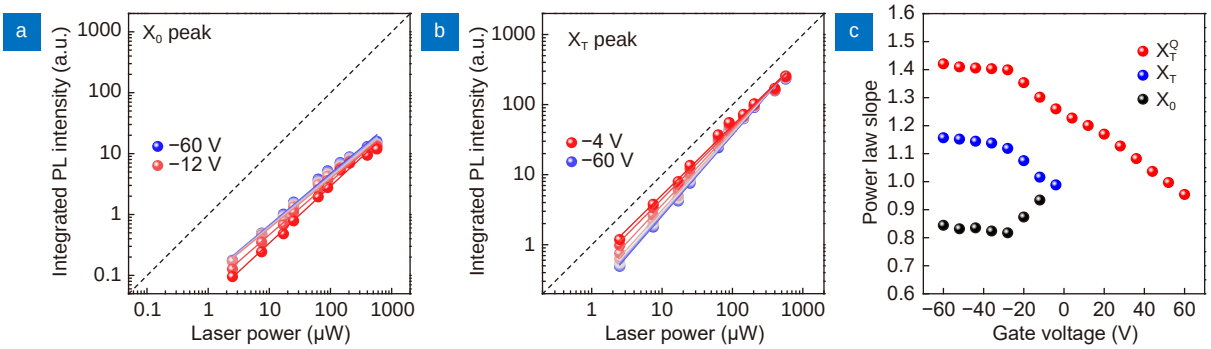

Fig. S2 | Power-law slope of X_0, X_T and X_T^Q at different back gate voltages. (**a**) Log-log plot of the integrated PL intensity for X_0 peak as a function of excitation power from –60 V to –12 V. Note that the X_0 peak could not be observed at gate from –4 V to 60 V. (**b**) Log-log plot of the integrated PL intensity for X_T peak as a function of excitation power from –60 V to –4 V. Note that the X_T peak could not be observed at gate from 4 V to 60 V. (**c**) Statistics of the power law slope for X_0, X_T and X_T^Q at each gate voltage. Note that the X_0 and X_T peak was too weak to be resolved at low powers and positive back-gate voltages.

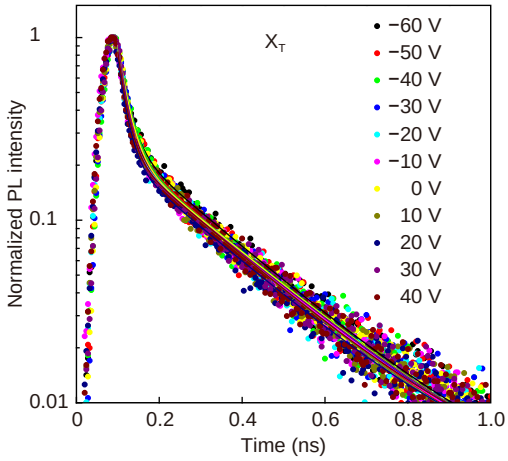

Fig. S3 | Gate-dependent time-resolved PL measurement for the X_T. Measured time-resolved PL traces (dots) and corresponding double exponential fitting (solid curves) for the X_T at different back-gate voltages (from –60 V to 40 V). The signal was too weak to be detected when the back-gate voltage exceeded 40 V.

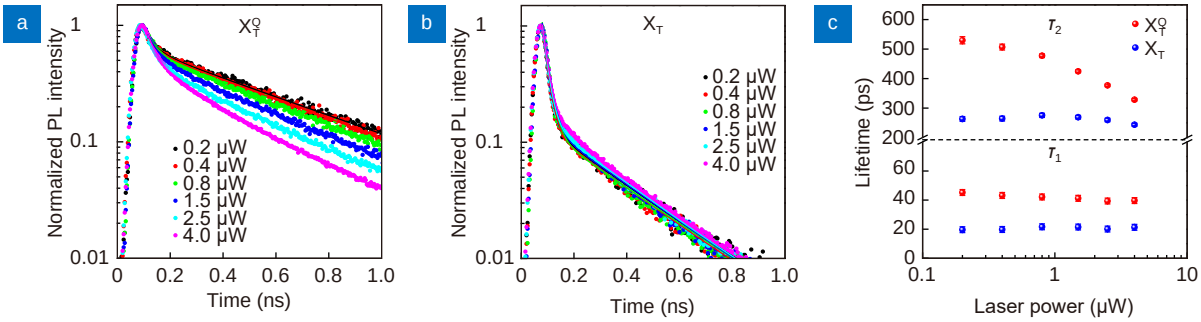

Fig. S4 | Excitation power-dependent time-resolved PL measurement for the X_T and X_T^Q. (**a**) Measured time-resolved PL traces (dots) and corresponding double exponential fitting (solid curves) for the X_T^Q at different excitation laser powers (from 0.2 μW to 4 μW). (**b**) Measured time-resolved PL traces (dots) and corresponding double exponential fitting (solid curves) for the X_T at different excitation laser powers. (**c**) The statistical values of the fast decay lifetime τ_1 and slow decay lifetime τ_2 for the fitting results of X_T and X_T^Q at different excitation laser powers.

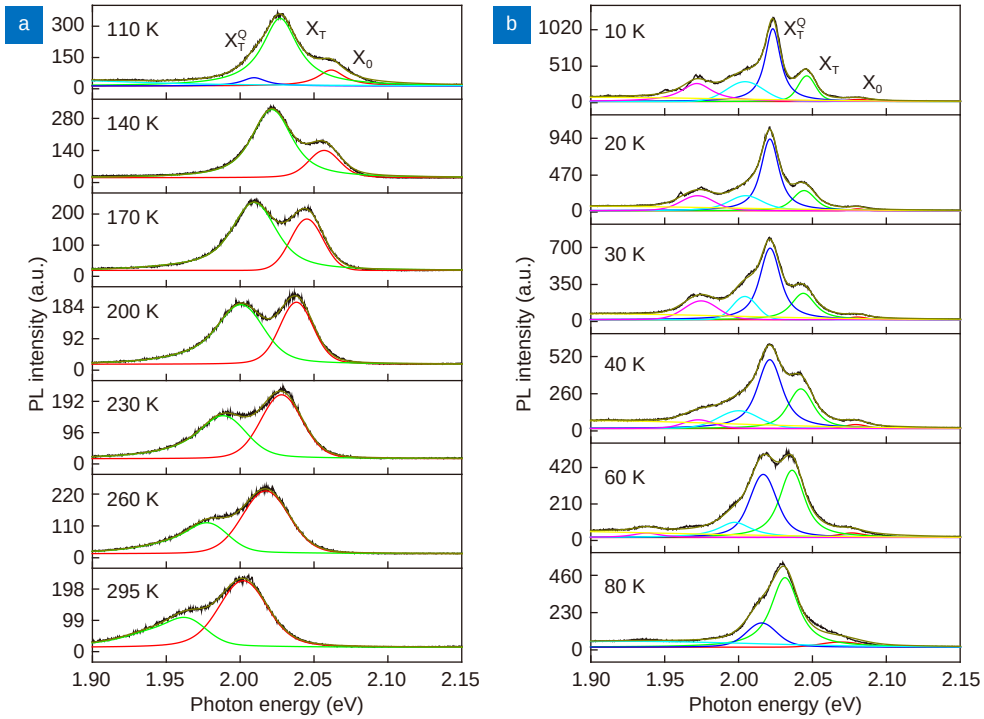

Fig. S5 | Fitting result of the temperature-dependent PL spectra of the monolayer WS_2. (**a**) Fitting results of the PL spectra from 295 K to 110 K temperatures with Voigt function. (**b**) Fitting results of the PL spectra from 80 K to 10 K temperatures with Voigt function.

Section 1: Thermal dynamic of neutral and charged excitons

Firstly, we determine the relative intensity of the neutral and charged excitonic species based on the Mass action model[S1]. From charge conservation of the photoexcited electrons and holes, the concentration of neutral states (n_X), charged states (n_{X^-}), free electrons (n_e), laser intensity (n_P), and doping level (n_B) have the following relationship:

$$n_P = n_X + n_{X^-} \ ,$$

$$n_B = n_e + n_{X^-} \ ,$$

$$n_e + n_X + 2n_{X^-} = n_P + n_B \ .$$

Then, the equilibrium populations for the species are governed by the Saha equation:

$$\frac{n_X n_e}{n_{X^-}} = Ak_B T\exp\left(-\frac{E_T}{k_B T}\right) = n_A \ ,$$

where k_B is Boltzmann constant, T is the temperature, E_T is the trion binding energy, $A = \frac{4M_X m_e}{\pi\hbar^2 M_{X^-}} \approx 6.18 \times 10^{11}$, n_A represents the temperature dependent equilibrium constant.

Solving the above equations gives:

$$\begin{cases} n_X = \frac{1}{2}\left(n_P - n_B - n_A + \sqrt{(n_P + n_B + n_A)^2 - 4n_P n_B}\right) \\ n_{X^-} = \frac{1}{2}\left(n_P + n_B + n_A - \sqrt{(n_P + n_B + n_A)^2 - 4n_P n_B}\right) \end{cases} .$$

This fits well with a two-level system such as the monolayer $MoSe_2$[S1]. However, due to the existence of dark states in the monolayer WS_2, both their populations will split into substructures:

$$n_X = n_{X_0} + n_{X_D} \ ,$$

$$n_{X^-} = n_{X_T} + n_{X_T^Q} \ ,$$

where n_{X_0} represents the bright exciton, n_{X_D} represents the dark exciton, n_{X_T} and $n_{X_T^Q}$ represent the two types of charged excitons, respectively. Resulting from the difference of energy levels between two states, their concentrations are

governed by the Boltzmann distribution[S2]:

$$\begin{cases} n_{X_0} = n_X \dfrac{\exp\left(-\dfrac{\Delta_1}{k_B T}\right)}{1+\exp\left(-\dfrac{\Delta_1}{k_B T}\right)} \text{const} \\ n_{X_T} = n_{X^-} \dfrac{\exp\left(-\dfrac{\Delta_2}{k_B T}\right)}{1+\exp\left(-\dfrac{\Delta_2}{k_B T}\right)} \text{const} \end{cases},$$

where Δ_1 represents the energy difference between two exciton levels, Δ_2 represents the energy difference between two trion levels.

At elevated temperatures, the value of Q-K valley energy difference (ΔE_{QK}) changes mainly due to the thermalization induced band renormalization[S3] that switches the population of X_T and X_T^Q. Thus, the concentration of X_T should be corrected with a temperature-related function ΔE_{QK} and becomes:

$$n_{X_T} = n_{X^-} \frac{\exp\left(-\dfrac{\Delta_2 - \Delta E_{QK}}{k_B T}\right)}{1+\exp\left(-\dfrac{\Delta_2 - \Delta E_{QK}}{k_B T}\right)} \text{const},$$

and the population of X_T^Q becomes:

$$n_{X_T^Q} = n_{X^-} \frac{1}{1+\exp\left(-\dfrac{\Delta_2 - \Delta E_{QK}}{k_B T}\right)} \text{const},$$

based on the conservation of total population $n_{X^-} = n_{X_T} + n_{X_T^Q}$. The ΔE_{QK} could be fit to a function $\Delta E_{QK} = a + b(k_B T)^2$, where a and b were fit to 15 and 0.24, respectively. The calculated results are shown in the figure below.

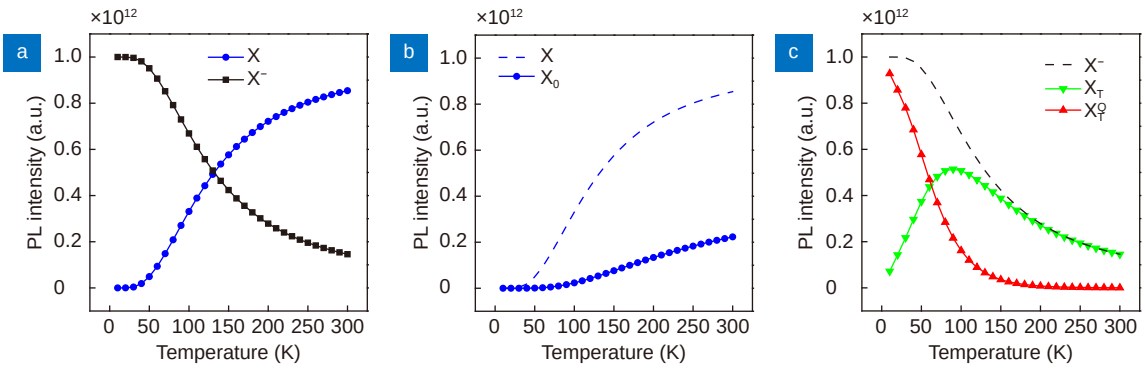

Fig. S6 | Calculated temperature-dependent PL intensity for the emission species. (**a**) The population of neutral and charged states without energy splitting. (**b**) The population of bright exciton (blue circle line) and the original neutral exciton (blue dashed line). (**c**) The population of X_T and X_T^Q (green and red lines) splitted from the original negatively charged exciton (black dashed line). The amount of absorbed photons is set as 1×10^{12} cm^{-2} for calculation, with an initial doping level 1×10^{12} cm^{-2}.

Section 2: Distribution of trions at different doping density

The Fermi energy (E_F) increases as the doping density is increased [4], and the concentration of Q valley electrons increases accordingly. The formation of Q-valley trion relies on the relative position between the Fermi energy and the Q valley energy level. When the Q valley energy level changes, the proportion of trions changes accordingly. We set the initial Fermi level at the bottom of the K valley, then the relative position between the Fermi energy and the Q valley energy level becomes: $\Delta E_F - \Delta E_{QK}$, where ΔE_{QK} is the Q-K valley energy difference, ΔE_F is the change of Fermi energy as a function of back-gate voltage. Then, the proportion of X_T and X_T^Q as a function of gate voltage increase could be calculated based on the Boltzmann distribution:

$$\frac{n_{X_T}}{n_{X_T^Q}} = \exp\left(-\frac{\Delta_2 + \Delta E_F - \Delta E_{QK}}{k_B T}\right),$$

with the addition of hole conservation relationship: $n_{X_T} + n_{X_T^Q} = n_{X-}$, we have:

$$\begin{cases} n_{X_T} = n_{X-} \dfrac{\exp\left(-\dfrac{\Delta_2 + \Delta E_F - \Delta E_{QK}}{k_B T}\right)}{1 + \exp\left(-\dfrac{\Delta_2 + \Delta E_F - \Delta E_{QK}}{k_B T}\right)} \text{const} \\ n_{X_T^Q} = n_{X-} \dfrac{1}{1 + \exp\left(-\dfrac{\Delta_2 + \Delta E_F - \Delta E_{QK}}{k_B T}\right)} \text{const} \end{cases},$$

Here Δ_2 is energy difference of two types of trions at zero doping.

The Fermi energies at different doping density are estimated based on the energy separation (ΔE_{X-T}) between neutral (X) and charged state (X^-). According to the energy and momentum conservation relationship of X and X^- in ref[S4], we have $\Delta E_{X-X^-} = \Delta E^0_{X^-} + \alpha \Delta E_F$, where $\Delta E^0_{X^-}$ is the energy separation of X and X^- at zero doping, α is a constant. Here in our estimation, the calculated curves match well with the experimental data (main Fig. 2(c)) when the α=0.5. Thus, we have $\Delta E_F = 2(\Delta E_{X-X^-} - \Delta E^0_{X^-})$. The Fermi energy as a function of gate voltage is shown below.

According to the gate sweep, the back gate induced carrier density doping n can be estimated using the parallel-plate

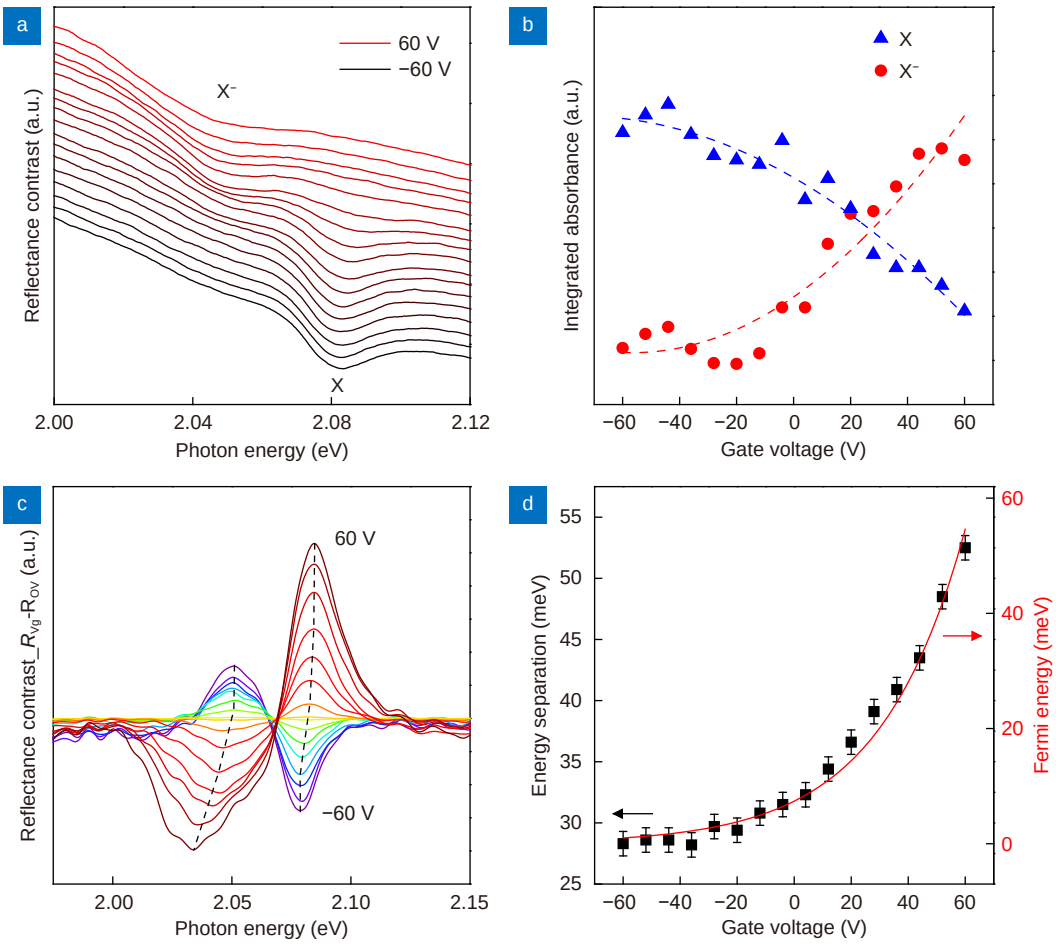

Fig. S7 | gate-dependent reflectance contrast spectra of monolayer WS_2 at *T*=10 K. (**a**) Reflectance contrast spectra for the monolayer WS_2 at 10 K with back gate voltages from –60 V to 60 V. The spectra are vertically shifted for clarity. (**b**) Integrated absorbance for the neutral and charged states. The dashed lines are fitting curves showing the trend. (**c**) The relative reflectance contrast spectra by subtracting the 0 V spectrum (R_{0V}) at each gate voltage (R_{Vg}) from (a). The peak intensities of the spectra are vertically expanded for clarity. (**d**) Energy separation of X and X^- at different gate voltages extracted from (c). The red curve is exponential fit with y=7.39e$^{0.033x}$ for the Fermi energy at each gate voltage.

capacitor model $n = C_{ox}\left(V_{bg} - V_{bg,th}\right)/e$, where V_{bg} is the back gate voltage, $V_{bg,th}$ is the threshold voltage, e is the unit charge, C_{ox} is the dielectric capacitance per unit area, which could be calculated from $C_{ox} = \varepsilon_0\varepsilon_r/d_{ox}$, where ε_0 is the dielectric constant of vacuum, ε_r is the relative dielectric constant (3.9) of SiO_2, d_{ox} is the thickness (300 nm) of SiO_2. The carrier density is estimated to be ~0.7×10^{12} cm^{-2} per 10 V. The transition trend of gate-dependent neutral and charged excitons used for the calculation is based on the fitting curves in Fig. S7(b) with the order of magnitude 10^{12} cm^{-2}. The amount of absorbed photons is set as 6×10^{12} cm^{-2} for calculation. The initial doping level is set as 1×10^{12} cm^{-2}. For the calculation in Fig. S8, the energy range of ΔE_{QK} is set from −200 to 200 meV, and the change of Fermi energy is from 0 to 60 meV. The Fermi level at zero gate voltage is set to at the bottom of the conduction band edge. For the Q valley energy levels of different TMDs, the ΔE_{QK} could be extracted from the density functional theory calculation[S5], as indicated in Fig. S8(a, b) with dashed lines. The cross-sections of the image are shown in Fig. S8(c–f), which agrees well with the experimental observations. It should be noted that for a sample with high initial doping, the population of trions would not be zero even applied with −60 V gate voltage, which is the case of our sample shown in main Fig. 2(c).

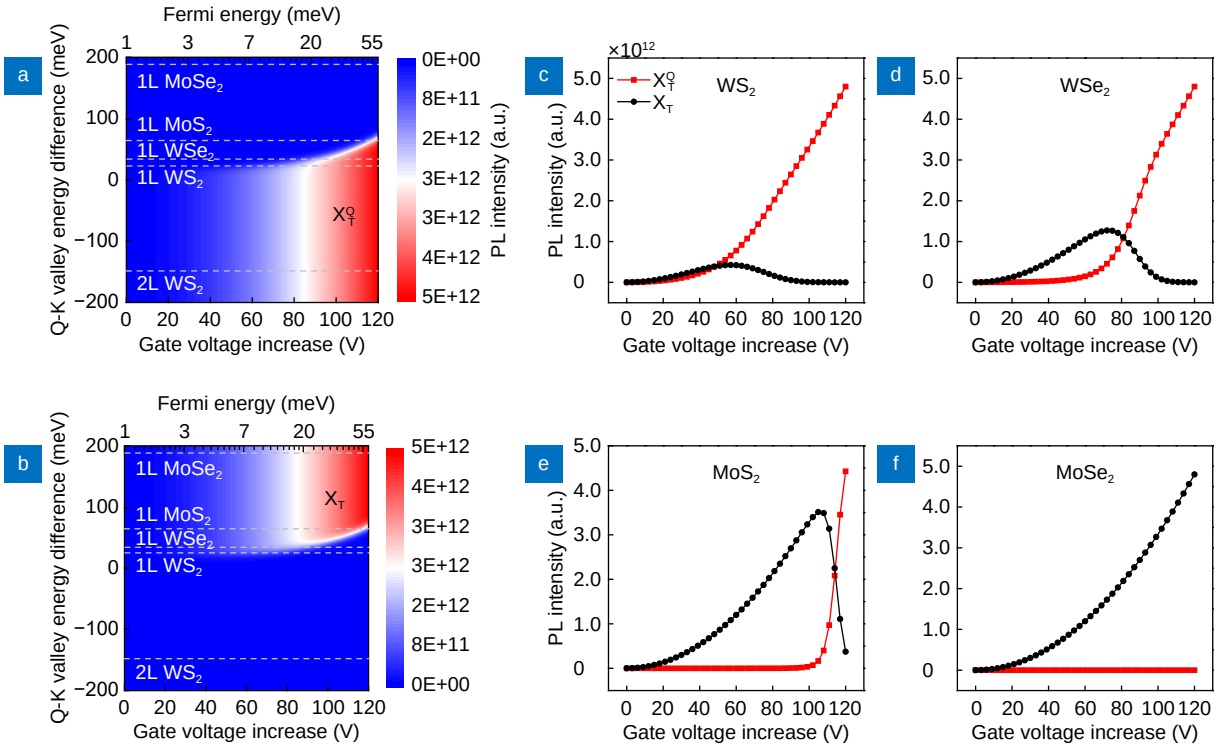

Fig. S8 | Calculated gate-dependent PL emissions of the trions X_T and X_T^Q for different TMDs. (**a**, **b**) Calculated population of X_T^Q and X_T as a function of gate voltage and the Q-K valley energy difference. The four types of TMDs with different Q-K valley splitting energies are indicated with dashed lines. (**c–f**) The transition curves of the X_T^Q and X_T as a function of gate voltage at the cross sections in (a) and (b). We found that the calculated result for 1L WSe_2 is in good agreement with the experimental result in Ref [6]. For 1L MoS_2 and $MoSe_2$, the Q valleys have higher energy level that are more difficult to access by back gate tuning.

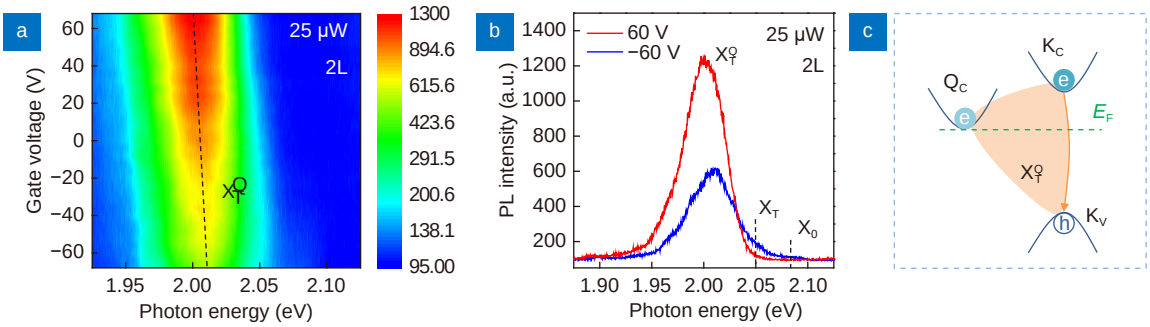

Fig. S9 | Gate-dependent PL spectra of a bilayer WS_2. (**a**) Color plot of the measured PL spectra for bilayer WS_2 as a function of back gate voltage at 25 μW excitation power at 10 K. The dashed line is guide to the eye showing the position of the emission peak. (**b**) PL spectra of bilayer WS_2 at –60 V and 60 V back gate voltage. (**c**) Schematic illustration of the Q-K valley energy difference for the bilayer WS_2 and the corresponding carrier relaxation pathways.

References

S1. Ross JS, Wu SF, Yu HY, Ghimire NJ, Jones AM et al. Electrical control of neutral and charged excitons in a monolayer semiconductor. *Nat Commun* **4**, 1474 (2013).

S2. Zhang XX, You YM, Zhao SYF, Heinz TF. Experimental evidence for dark excitons in monolayer WSe_2. *Phys Rev Lett* **115**, 257403 (2015).

S3. Peng GH, Lo PY, Li WH, Huang YC, Chen YH et al. Distinctive signatures of the spin- and momentum-forbidden dark exciton states in the photoluminescence of strained WSe_2 monolayers under thermalization. *Nano Lett* **19**, 2299–2312 (2019).

S4. Chernikov A, Van Der Zande AM, Hill HM, Rigosi AF, Velauthapillai A et al. Electrical tuning of exciton binding energies in monolayer WS_2. *Phys Rev Lett* **115**, 126802 (2015).

S5. Roldán R, Silva-Guillén JA, López-Sancho MP, Guinea F, Cappelluti E et al. Electronic properties of single-layer and multilayer transition metal dichalcogenides MX_2 (M = Mo, W and X = S, Se). *Ann Phys* **526**, 347–357 (2014).

S6. Jones AM, Yu HY, Ghimire NJ, Wu SF, Aivazian G et al. Optical generation of excitonic valley coherence in monolayer WSe_2. *Nat Nanotechnol* **8**, 634–638 (2013).